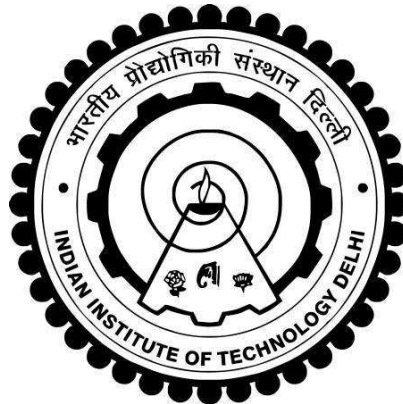


**MODELLING, ANALYSIS AND IMPLEMENTATION OF  
A SWITCHED RELUCTANCE MACHINE BASED WIND  
ENERGY CONVERSION SYSTEM**

**SWAGATA MAPA**



**DEPARTMENT OF ELECTRICAL ENGINEERING  
INDIAN INSTITUTE OF TECHNOLOGY DELHI  
JULY 2022**



© Indian Institute of Technology Delhi (IITD), New Delhi, 2022



**MODELLING, ANALYSIS AND IMPLEMENTATION OF  
A SWITCHED RELUCTANCE MACHINE BASED WIND  
ENERGY CONVERSION SYSTEM**

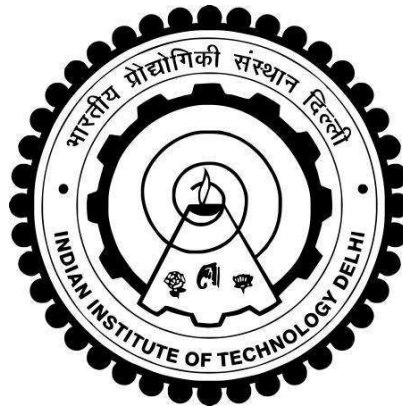
by

**SWAGATA MAPA**

**Department of Electrical Engineering**

*Submitted*  
*in fulfilment of the requirements of the degree of*  
**DOCTOR OF PHILOSOPHY**

to the



**INDIAN INSTITUTE OF TECHNOLOGY DELHI**

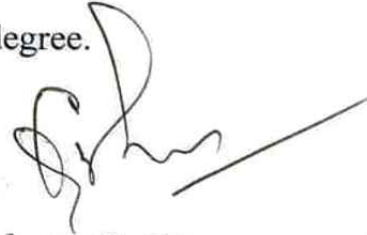
**JULY 2022**



## CERTIFICATE

This is to certify that the dissertation titled “**Modelling, Analysis and Implementation of a Switched Reluctance Machine Based Wind Energy Conversion System**”, being submitted by **Ms. Swagata Mapa** to the Department of Electrical Engineering, Indian Institute of Technology Delhi, for the award of the degree of Doctor of Philosophy, is a record of the bonafide research work carried out by her under my guidance and supervision.

**Ms. Swagata Mapa** has fulfilled the requirements for the submission of this thesis, which to my knowledge has reached the requisite standard. The results obtained herein have not been submitted in part or in full to any other University or Institute for the award of any degree.



Professor **G. Bhuvaneswari**

Department of Electrical Engineering  
Indian Institute of Technology Delhi  
New Delhi-110016, India

Date: 08/07/2022



## ACKNOWLEDGEMENTS

At the outset, I would like to express my heartfelt thanks to the almighty for blessing me with this much awaited day when I have finally got the opportunity to pen down my feelings of gratitude and accomplishment to mark the culmination of this wonderful five-year long journey.

My foremost and deepest gratitude to **Prof. G. Bhuvaneswari** for not only being my PhD supervisor, but also my mentor and a great pillar of strength. Working under her supervision has been a privilege and honour. Her resourceful inputs, excellent foresight, willingness to pay heed to my ideas and complementing them with her thoughtful suggestions, have been immensely useful during my course of research. I am grateful and deeply indebted to her for constantly motivating and imbibing in me the true research acumen. I have been genuinely blessed to have her in a pivotal role in this ‘wonderful’ journey.

I would also like to sincerely thank all the SRC members **Prof. Bhim Singh, Dr. Anandarup Das, and Dr. Ashu Verma** for providing me their valuable insights, suggestions and encouragement throughout my research work. I would also like to thank my ex-co-guide **Dr. Ramkrishan Maheswari**.

I am thankful to IIT Delhi for providing the research facilities. Thanks are due to **Sh. Srichand, Sh. Puran Singh, Sh. Jitendra Kumar, Sh. Anurag and Sh. Rahul** of PG Machines Lab and Departmental Workshop, IIT Delhi, for their sustained help to carry out my experimental work during the course of my doctoral studies.

My journey at IIT Delhi would have been incomplete without the wonderful camaraderie that I shared with some of my research scholar and M.Tech friends. I would like to extend special thanks to my fellow research scholars **Dr. Sreejith Ravindran, Dr. Nibedita Parida, Dr. Deepu Vijay M, Dr. Pradyumna Ranjan Ghosh, Dr. Poonam Jayal, Ms. Samiksha Rawat, Mr. Saurabh Shukla, Mr. Sukrashis Sarkar, Mr. Ebin Mathew and Mr. V. Goutham** for their indispensable technical as well as moral support. I would also like to thank my friends, **Ms. Nidhi Bisht, Ms. Dipta Choudhuri, Mr. Rahul Sharma and Mr. Rajat** for their **encouragement and support**.

This long journey would have been impossible without the love and support of my husband, my parents and other family members.



(Swagata Mapa)

New Delhi.

2017EEZ8160

## ABSTRACT

Electricity generation from renewables has become a hot topic of research in the last couple of decades since renewable energy sources are visualised as one of the powerful means to fight global warming and climate change. Electrical power generation from wind energy has seen considerable growth in the last twenty years. Both off-shore and on-shore wind energy conversion system (WECS) configurations have gained equal importance. The major electrical components involved with WECS, such as generators and power converters, have gone through several important transformations in their structural and control aspects. Conventionally doubly fed induction generators (DFIGs) have been in use for generating hundreds of kilowatts of power from wind due to their lower cost, which can be attributed to their capability to function with partial rated power converters. However, DFIGs are not as rugged as the squirrel cage induction generators. In this regard, permanent magnet synchronous generators (PMSGs) with full-rated converters could work extremely efficiently and reliably as wind power generators, especially at MWs of power levels. But, the presence of a permanent magnet in the rotor makes PMSGs really expensive and heavy. For small-scale WECS like the ones installed on the roof-top, some of the special electrical machines such as switched reluctance machines (SRMs) and permanent magnet brushless DC machines (PMBLDCMs) can be employed. This thesis explores the possibility of using an SRM for a small-scale wind power generating system.

SRM has several advantages like high torque to inertia ratio, better reliability, maintenance-free operation and rugged rotor structure devoid of permanent magnets and

windings. It is also more cost effective than a PMSG. One of the major problems associated with the SRM is the ripples present in its output power. When an SRM based WECS has to be implemented, it would be desirable to model the entire system in a simulation tool and verify its successful working through simulation studies. For this purpose, it is essential to develop an accurate model for the SRM. Due to its non-linear magnetic behaviour, modelling an SRM is a formidable task. An attempt has been made in this thesis to develop two different models for a 1-hp 8/6 SRM by making use of the experimentally obtained flux linkage characteristics, for different phase currents and rotor positions. One is a linear model wherein the inductance is represented by mathematical equations depending upon the rotor position and phase currents. The other one is a non-linear model where the flux linkage is represented by making use of look-up tables and/or a polynomial function consisting of rotor position and phase current. These developed models have been validated by simulating the motoring and generating modes of operation and comparing the performances obtained with the actual experimental results. The results are found to match well with each other which verifies that the models developed represent the machine reasonably accurately.

A small-scale WECS based on an SRM can be used advantageously to generate electricity to cater to the needs of remote areas where grid connectivity is completely absent or unreliable. If the machine can work in self-excited mode, that would be highly beneficial. Finding an appropriate value of capacitance for the self-excited operation of an SRM over a wide range of wind-speeds has been taken up as the second task in this research work. It is shown that by choosing the capacitor value judiciously, and by providing a small

voltage initially across the capacitor, voltage is built-up properly in the phase winding of the switched reluctance generator (SRG). The functioning of SRG in self-excited mode has been demonstrated for a wide range of wind speeds in simulation studies as well as in the experimental setup.

Harvesting maximum power from a roof-top WECS (as per the wind speed) is extremely important as these systems are designed for meagre power ratings and also to make a household electrically self-sufficient. Maximum power point tracking (MPPT) control for the SRG is done through an outer power control loop and an inner current control loop. Current control is accomplished by choosing the firing angles for the devices in the asymmetric half bridge converter (AHBC) suitably. Two different optimization techniques, namely, particle swarm optimization technique and gravitational search algorithm are used to arrive at the optimum combination of firing angles to extract maximum power from the SRG at different wind speeds. These optimization techniques are capable of finding appropriate combinations of firing angles even without having prior knowledge of SRM's geometrical parameters like rotor and stator pole widths, interpolar space width, length of the air gap, etc. Modelling and simulation of these optimization algorithms applied to an SRG based WECS have been carried out in the Simulink/MATLAB environment. Finally, in the experimental setup, MPPT has been achieved for varying wind speed conditions by making use of these turn-on and turn-off angles for the AHBC devices.

Due to varying values of wind velocity, the DC output voltage from an SRG based WECS does not remain constant. A DC-DC converter is used at the output of the SRG to regulate

its output voltage before feeding it to the loads/ DC microgrid. Non-isolated topologies are preferred over isolated and interleaved configurations, as the focus here is on low cost and a compact system. A SEPIC (Single ended primary inductor converter) is used to regulate the output voltage of the SRG before tying it up to a 48 V DC bus to which a battery energy storage system and loads of a DC home are connected. The entire system has been modelled and simulated and found to perform satisfactorily. A laboratory prototype consisting of a self-excited SRG driven by a DC motor (emulating a wind turbine), an AHBC, a SEPIC to regulate the DC voltage, along with a battery energy storage system (BESS) and loads, has been developed and its performance has been studied at different prime-mover speeds. It is found that the voltage output from the SRG is regulated to 48 V under varying wind speeds and simultaneously, maximum power extraction is accomplished. When the load demand exceeds the generation, BESS makes up for the short-fall. When the wind speed is higher and the load demand is lower, BESS makes use of the excess generated power to replenish its charge.

To summarize, a self-excited SRG based wind energy conversion system has been designed, modelled, analyzed, simulated and implemented in hardware to deliver a regulated DC voltage of 48 V magnitude to a small microgrid consisting of a BESS and various loads, at varying wind velocity conditions.

## सार

नवीकरणीय ऊर्जा से बिजली उत्पादन पिछले कुछ दशकों में अनुसंधान का एक गर्म (बहुचर्चित) विषय बन गया है क्योंकि अक्षय ऊर्जा स्रोतों को ग्लोबल वार्मिंग और जलवायु परिवर्तन से लड़ने के शक्तिशाली साधनों में से एक के रूप में देखा जाता है। पवन ऊर्जा से विद्युत उत्पादन में पिछले बीस वर्षों में काफी वृद्धि देखी गई है। अपतटीय और तटवर्ती पवन ऊर्जा रूपांतरण प्रणाली (WECS) दोनों विन्यासों को समान महत्व प्राप्त हुआ है। WECS से जुड़े प्रमुख विद्युत घटक, जैसे जनरेटर और पावर कन्वर्टर्स, अपने संरचनात्मक और नियंत्रण पहलुओं में कई महत्वपूर्ण परिवर्तनों से गुजरे हैं। परंपरागत रूप से डबल फीडेड इंडक्शन जेनरेटर (डीएफआईजी) अपनी कम लागत के कारण हवा से सैकड़ों किलोवाट बिजली पैदा करने के लिए उपयोग में हैं, जिसे आंशिक रेटेड पावर कन्वर्टर्स के साथ काम करने की उनकी क्षमता के लिए जिम्मेदार ठहराया जा सकता है। हालाँकि, DFIGs गिलहरी (स्क्रिरेल) केज इंडक्शन जेनरेटर की तरह बीहड़ (विषम परिस्थिति में चलने के लिए) नहीं होते हैं। इस संबंध में, पूर्ण-रेटेड कन्वर्टर्स के साथ स्थायी चुंबक सिंक्रोनस जेनरेटर (पीएमएसजी) पवन ऊर्जा जनरेटर के रूप में बेहद कुशलतापूर्वक और भरोसेमंद काम कर सकते हैं, खासकर बिजली के स्तर के मेगावाट पर। लेकिन, रोटर में स्थायी चुंबक की उपस्थिति PMSG को वास्तव में महंगा और भारी बनाती है। छोटे पैमाने के WECS जैसे रूफ-टॉप पर स्थापित कुछ विशेष विद्युत मशीनों जैसे स्विच रिलक्टेंस मशीन (SRMs) और स्थायी चुंबक ब्रशलेस DC मशीन (PMBLDCM) को नियोजित (कार्यरत) किया जा सकता है। यह थीसिस एक छोटे पैमाने

पर पवन ऊर्जा उत्पादन प्रणाली के लिए एसआरएम का उपयोग करने की संभावना की पड़ताल करती है।

एसआरएम के कई फायदे हैं जैसे उच्च टोर्क से जड़ता अनुपात, बेहतर विश्वसनीयता, रखरखाव मुक्त संचालन और स्थायी चुंबक और घुमाव से रहित मजबूत रोटर संरचना। यह PMSG की तुलना में अधिक लागत प्रभावी भी है। SRM से जुड़ी प्रमुख समस्याओं में से एक इसकी आउटपुट पावर में मौजूद तरंगें हैं। जब एक एसआरएम आधारित डब्ल्यूईसीएस को लागू किया जाना है, तो यह वांछनीय होगा कि पूरी प्रणाली को एक सिमुलेशन टूल में मॉडल किया जाए और सिमुलेशन अध्ययनों के माध्यम से इसके सफल कामकाज को सत्यापित किया जाए। इस प्रयोजन के लिए एसआरएम के लिए एक सटीक मॉडल विकसित करना आवश्यक है। अपने गैर-रैखिक (नॉन-लीनियर) चुंबकीय व्यवहार के कारण, एक एसआरएम मॉडलिंग एक कठिन कार्य है। इस थीसिस में विभिन्न चरण धाराओं और रोटर स्थितियों के लिए प्रयोगात्मक रूप से प्राप्त फ्लक्स लिंकेज विशेषताओं (विशिष्ट गुण) का उपयोग करके 1-एचपी 8/6 एसआरएम के लिए दो अलग-अलग मॉडल विकसित करने का प्रयास किया गया है। एक रैखिक (लीनियर) मॉडल है जिसमें रोटर की स्थिति और चरण धाराओं के आधार पर गणितीय समीकरणों द्वारा अधिष्ठापन का प्रतिनिधित्व किया जाता है। दूसरा एक गैर-रैखिक (नॉन-लीनियर) मॉडल है जहां फ्लक्स लिंकेज को लुक-अप टेबल और/या रोटर स्थिति और चरण वर्तमान से युक्त बहुपद फंक्शन का उपयोग करके दर्शाया जाता है। इन विकसित मॉडलों को मोटरिंग का अनुकरण और संचालन के तरीके उत्पन्न करके और वास्तविक प्रयोगात्मक परिणामों के साथ प्राप्त प्रदर्शन की तुलना करके मान्य किया गया है।

परिणाम एक दूसरे के साथ अच्छी तरह मेल खाते हुए पाए जाते हैं जो यह सत्यापित करता है कि विकसित मॉडल मशीन का यथोचित सटीक प्रतिनिधित्व करते हैं।

एसआरएम पर आधारित एक छोटे पैमाने के डब्ल्यूईसीएस का उपयोग बिजली पैदा करने के लिए लाभकारी रूप से किया जा सकता है ताकि दूरदराज के क्षेत्रों की जरूरतों को पूरा किया जा सके जहां ग्रिड कनेक्टिविटी पूरी तरह से अनुपस्थित या अविश्वसनीय है। अगर मशीन सेल्फ एक्साइटेड मोड में काम कर सकती है, तो यह बेहद फायदेमंद होगा। इस शोध कार्य में दूसरे कार्य के रूप में हवा की गति की एक विस्तृत श्रृंखला पर एक एसआरएम के आत्म-उत्तेजित (सेल्फ एक्साइटेड) संचालन के लिए समाई (कपैसिटर) का उचित मूल्य ढूँढना लिया गया है। यह दिखाया गया है कि संधारित्र मूल्य को विवेकपूर्ण ढंग से चुनकर, और संधारित्र में शुरू में एक छोटा वोल्टेज प्रदान करके, स्विच किए गए अनिच्छा जनरेटर (एसआरजी) के चरण घुमावदार में वोल्टेज ठीक से बनाया गया है। स्व-उत्तेजित मोड में एसआरजी के कामकाज को सिमुलेशन अध्ययनों के साथ-साथ प्रयोगात्मक सेटअप में हवा की गति की एक विस्तृत श्रृंखला के लिए प्रदर्शित किया गया है।

रूफ-टॉप WECS (हवा की गति के अनुसार) से अधिकतम बिजली का संचयन अत्यंत महत्वपूर्ण है क्योंकि इन प्रणालियों को कम बिजली रेटिंग के लिए डिज़ाइन किया गया है और एक घर को विद्युत रूप से आत्मनिर्भर बनाने के लिए भी। एसआरजी के लिए अधिकतम पावर प्वाइंट ट्रैकिंग (एमपीपीटी) नियंत्रण एक बाहरी पावर कंट्रोल लूप और एक आंतरिक करंट कंट्रोल लूप के माध्यम से किया जाता है। असममित आधा पुल कनवर्टर (हाफ ब्रिज कनवर्टर) (एएचबीसी) में उपकरणों के लिए फायरिंग कोणों को उपयुक्त रूप से चुनकर वर्तमान नियंत्रण पूरा किया जाता है। दो अलग-अलग अनुकूलन तकनीकों, अर्थात् कण झुंड अनुकूलन (पार्टिकल स्वार्म ऑप्टिमाइजेशन) तकनीक

और गुरुत्वाकर्षण खोज एल्गोरिदम का उपयोग विभिन्न हवा की गति पर एसआरजी से अधिकतम शक्ति निकालने के लिए फायरिंग कोणों के इष्टतम संयोजन पर पहुंचने के लिए किया जाता है। ये अनुकूलन तकनीक एसआरएम के ज्यामितीय मापदंडों जैसे रोटर और स्टेटर पोल की चौड़ाई, अंतर-ध्रुवीय स्थान की चौड़ाई, हवा के अंतराल की लंबाई आदि के पूर्व ज्ञान के बिना भी फायरिंग कोणों के उपयुक्त संयोजन खोजने में सक्षम हैं। इन अनुकूलन एल्गोरिदम का मॉडलिंग और अनुकरण लागू किया गया एक SRG आधारित WECS को सिमुलिक/MATLAB वातावरण में किया गया है। अंत में, प्रायोगिक सेटअप में, एमपीपीटी को एचबीसी उपकरणों के लिए इन टर्न-ऑन और टर्न-ऑफ कोणों का उपयोग करके हवा की गति की बदलती स्थितियों के लिए हासिल किया गया है।

हवा के वेग के अलग-अलग मूल्यों के कारण, एसआरजी आधारित डब्ल्यूईसीएस से डीसी आउटपुट वोल्टेज स्थिर नहीं रहता है। डीसी-डीसी कनवर्टर का उपयोग एसआरजी के आउटपुट में लोड/डीसी माइक्रोग्रिड को फीड करने से पहले इसके आउटपुट वोल्टेज को विनियमित करने के लिए किया जाता है। गैर-पृथक टोपोलॉजी को पृथक और इंटरलीव्ड कॉन्फिगरेशन पर पसंद किया जाता है, क्योंकि यहां फोकस कम लागत और एक कॉम्पैक्ट सिस्टम पर है। एक SEPIC (सिंगल एंडेड प्राइमरी इंडक्टर कनवर्टर) का उपयोग SRG के आउटपुट वोल्टेज को नियंत्रित करने के लिए 48 V DC बस से जोड़ने से पहले किया जाता है, जिसमें एक बैटरी एनर्जी स्टोरेज सिस्टम और एक DC होम का लोड जुड़ा होता है। पूरी प्रणाली को मॉडल और अनुकरण किया गया है और संतोषजनक ढंग से प्रदर्शन करने के लिए पाया गया है। एक डीसी मोटर (एक पवन टरबाइन का अनुकरण), एक एचबीसी, एक बैटरी ऊर्जा भंडारण प्रणाली (बीईएस) और भार के साथ डीसी

वोल्टेज को विनियमित करने के लिए एक एसईपीआईसी द्वारा संचालित एक स्व-उत्तेजित (सेल्फ एक्साइटेड) एसआरजी से युक्त एक प्रयोगशाला प्रोटोटाइप विकसित किया गया है और इसके प्रदर्शन का विभिन्न प्राइम-मूवर गति पर अध्ययन किया गया है। यह पाया गया है कि एसआरजी से वोल्तेज आउटपुट को अलग-अलग हवा की गति के तहत 48 V तक नियंत्रित किया जाता है और साथ ही, अधिकतम बिजली निष्कर्षण पूरा किया जाता है। जब लोड की मांग पीढ़ी से अधिक हो जाती है, तो BESS कमी की भरपाई करता है। जब हवा की गति अधिक होती है और लोड की मांग कम होती है, तो बीईएसएस अपने चार्ज को फिर से भरने के लिए अतिरिक्त उत्पन्न बिजली का उपयोग करता है।

संक्षेप में, एक स्व-उत्तेजित (सेल्फ एक्साइटेड) एसआरजी आधारित पवन ऊर्जा रूपांतरण प्रणाली को हार्डवेयर में डिजाइन, मॉडल, विश्लेषण, सिमुलेटेड और कार्यान्वित किया गया है ताकि बीईएसएस (BESS) और विभिन्न भारों से युक्त एक छोटे माइक्रोग्रिड को 48 वी (V) परिमाण का एक विनियमित डीसी वोल्तेज अलग-अलग पर वितरित किया जा सके, हवा के वेग की स्थिति।

संक्षेप में, एक स्व-उत्तेजित (सेल्फ एक्साइटेड) एसआरजी आधारित पवन ऊर्जा रूपांतरण प्रणाली को हार्डवेयर में डिजाइन, मॉडल, विश्लेषण, सिमुलेटेड और कार्यान्वित किया गया है ताकि बीईएसएस (BESS) और विभिन्न भारों से युक्त एक छोटे माइक्रोग्रिड को 48 वी (V) परिमाण का एक विनियमित डीसी वोल्तेज अलग-अलग हवा के वेग की स्थिति पर वितरित किया जा सके।



# TABLE OF CONTENTS

Certificate	i
Acknowledgements	iii
Abstract	v
Table of Contents	xv
List of Figures	xix
List of Tables	xxiii
List of Abbreviations	xxv
List of Symbols	xxvii
<b>CHAPTER I INTRODUCTION</b>	<b>1-12</b>
1.1 General	1
1.2 State of the art	4
1.3 Objectives and Scope of work	6
1.4 Organization of the Thesis	9
<b>CHAPTER II LITERATURE REVIEW</b>	<b>13-28</b>
2.1 General	13
2.2 Developments in wind energy conversion systems	13
2.3 Switched reluctance machine: Modelling and Control aspects	17
2.4 Switched reluctance machine: Operation as a generator	20
2.5 SRG with DC-DC converters	24
2.6 Research gaps	26
2.7 Summary	27
<b>CHAPTER III SYSTEM CONFIGURATION</b>	<b>29-38</b>
3.1 General	29
3.2 System description for motoring operation of the SRM	29
3.3 System description for SRG operation driven by a wind turbine	32
3.4 SRG in self-excited mode with a DC-DC Converter	35
3.5 Summary	38
<b>CHAPTER IV MODELLING OF SRM</b>	<b>39-70</b>
4.1 General	39
4.2 Obtaining the parameters of an SRM through experimentation	39
4.2.1 Estimation of flux-linkage characteristics	40
4.2.2 Inductance Estimation	42
4.2.3 Torque Estimation	44
4.3 Model for an SRM assuming linear variation of inductance	47
4.4 Non-linear model for an SRM using $\varphi - i - \theta$ characteristics	51
4.5 Model for an SRM using a polynomial function for the phase inductance in terms of rotor position ' $\theta$ '	52

4.6	Model for an SRM using a polynomial function for the phase inductance in terms of ' $i$ ' and ' $\theta$ '	55
4.7	Simulation Results	56
4.7.1	Results of the non-linear model of the SRM	56
4.7.2	Results of the linear model of the SRM	60
4.7.3	Results of polynomial inductance model in terms of rotor position $\theta$	63
4.7.4	Results of polynomial inductance model (in terms of ' $i$ ' and ' $\theta$ ') for the SRM	66
4.8	Summary	70
<b>CHAPTER V SELF-EXCITATION OF AN SRG IN A WPGS</b>		<b>71-78</b>
5.1	General	71
5.2	Voltage build-up process in an SRG	71
5.3	Choice of capacitor for an SRG working in a specified range of speeds	73
5.4	Simulation results of the SRG with suitable choice of capacitor	75
5.5	Summary	77
<b>CHAPTER VI OPTIMIZATION TECHNIQUES FOR OBTAINING MAXIMUM POWER OUTPUT FROM AN SRG</b>		<b>79-102</b>
6.1	General	79
6.2	Dependency of maximum power on excitation voltage and conduction angles	79
6.2.1	Effect of varying $\theta_{on}$ and $\theta_{off}$ at constant excitation voltage	81
6.2.2	Effect of varying excitation voltage at constant $\theta_{on}$ and $\theta_{off}$	82
6.3	Meta-heuristic optimization algorithms	83
6.3.1	GSA	84
6.3.2	PSO	87
6.4	Simulation results with GSA and PSO in three different wind speeds	89
6.5	Performance of the self-excited SRG with different DC-DC converters at various wind speeds	93
6.6	Summary	101
<b>CHAPTER VII HARDWARE IMPLEMENTATION</b>		<b>103-116</b>
7.1	General	103
7.2	System description	103
7.2.1	Description of the SRM	105
7.2.2	Rotary Incremental encoder	106
7.2.3	DC Machine as a load or prime mover	109
7.2.4	DSP TMS320F28379D	109
7.2.5	Current sensor and voltage sensor boards	110
7.2.6	Converters	111
7.3	Summary	115
<b>CHAPTER VIII EXPERIMENTAL RESULTS</b>		<b>117-134</b>
8.1	General	117

8.2	Closed loop control of the SRM functioning as a motor	117
8.3	Closed loop control of switched reluctance generator	120
8.4	DC voltage regulation of the SRG with SEPIC	126
8.5	SRG connected to a DC microgrid with a BDC and a battery	131
8.6	Summary	133
<b>CHAPTER IX CONCLUSIONS</b>		<b>135-140</b>
9.1	General	135
9.2	Salient contributions of the research work	136
9.3	Future scope of Work	139
<b>REFERENCES</b>		<b>141-151</b>
<b>APPENDIX-A</b>		<b>153</b>
<b>APPENDIX-B</b>		<b>155</b>
<b>LIST OF PUBLICATIONS</b>		<b>157</b>
<b>BIO-DATA</b>		<b>159</b>



## LIST OF FIGURES

- Fig. 3.1 Control configuration of the switched reluctance machine in motoring mode
- Fig. 3.2 System Configuration (Generating condition of SRM)
- Fig. 3.3 Wind Turbine characteristics
- Fig. 3.4 SRG based WPGS with a DC-DC converter for regulating the output voltage
- Fig. 4.1 Waveforms of the gate pulse given to buck converter, phase voltage and phase current at:  
(a) aligned position ( $\theta = 30^\circ$ ), (b) unaligned ( $\theta = 0^\circ$ ) positions of the rotor
- Fig. 4.2 Flux obtained from terminal voltage and current of the phase winding by using Simpson's one-third rule
- Fig. 4.3 Flux linkage characteristics for varying ' $i$ ' and ' $\theta$ '
- Fig. 4.4 Inductance calculation from the flux linkage characteristics
- Fig. 4.5 Phase inductance profile
- Fig. 4.6 Co-energy and Torque calculations
- Fig. 4.7 Co-energy profile
- Fig. 4.8 Torque profile
- Fig. 4.9 Inductance profile introduced into the linear model
- Fig. 4.10 Models developed for the 8/6 SRM (Linear model based on the inductance profile)
- Fig. 4.11 Models developed for the 8/6 SRM (non-linear model based on the flux-linkage)
- Fig. 4.12 ITBL characteristics
- Fig. 4.13 Magnified view of the model for the SRM based on polynomial function of the inductance in terms of ' $\theta$ '
- Fig. 4.14 Responses of the non-linear model of the SRM drive for load perturbation (from 0.5 to 1 Nm at a speed of 209 rad/s) at 3 s and reference speed change (of 209 to 100 rad/s at 1 Nm load torque) at 6.5 s
- Fig. 4.15 Responses of the non-linear model of the SRM drive during regenerative braking (at 3 s, speed changed from 157 to 100 rad/s)
- Fig. 4.16 Responses (voltage, current, flux, speed, torque, generated power and mechanical input power) of the non-linear model of the SRG while being driven by a wind-turbine
- Fig. 4.17 Responses of the linear model of the SRM drive for a load perturbation (from 0.5 to 1 Nm at a speed of 209 rad/s) at 3 s and a reference speed change (of 209 to 100 rad/s at 1 Nm load torque) at 6.5 s
- Fig. 4.18 Responses of the linear model of the SRM drive during regenerative braking (at 3 s, the reference speed is changed from 157 rad/s to 100 rad/s)
- Fig. 4.19 Responses (voltage, current, flux, speed, torque, generated power and mechanical input power) of the linear model of the SRG while being driven by a wind-turbine

- Fig. 4.20 Responses of the polynomial inductance model (inductance variation with rotor position ' $\theta'$ ') of the SRM drive for a load perturbation (from 0.5 to 1 Nm at a speed of 209 rad/s) at 3 s and a reference speed change (of 209 to 100 rad/s at 1 Nm load torque) at 6.5 s
- Fig. 4.21 Responses of the polynomial inductance model (inductance variation with rotor position ' $\theta'$ ') of the SRM drive during regenerative braking (at 3 s, the reference speed is changed from 157 rad/s to 100 rad/s)
- Fig. 4.22 Responses (voltage, current, flux, speed, torque, generated power and mechanical input power) of the polynomial inductance model (inductance variation with rotor position ' $\theta'$ ') of the SRG while being driven by a wind-turbine
- Fig. 4.23 Responses of the polynomial inductance model (in terms of ' $i'$ ' and ' $\theta'$ ') of the SRM drive for a load perturbation (from 0.5 to 1 Nm at a speed of 209 rad/s) at 3 s and a reference speed change (of 209 to 100 rad/s at 1 Nm load torque) at 6.5 s
- Fig. 4.24 Responses of the polynomial inductance model (in terms of ' $i'$ ' and ' $\theta'$ ') of the SRM drive during regenerative braking (at 3 s, the reference speed is changed from 157 rad/s to 100 rad/s)
- Fig. 4.25 Responses (voltage, current, flux, speed, torque, generated power and mechanical input power) of the polynomial inductance model (in terms of ' $i'$ ' and ' $\theta'$ ') of the SRG while being driven by a wind-turbine
- Fig. 5.1 Variation of  $\frac{d\phi}{d\theta}$  with respect to current for aligned and unaligned rotor positions
- Fig. 5.2 Simulation responses (voltage (V), current (A), flux (V.s), speed (rad/s) and torque (Nm)) of the self-excited SRG at three different wind velocity conditions (7 m/s, 6 m/s and 5 m/s) and (right side) magnified view of voltage, current and flux at transient condition
- Fig. 5.3 Voltage (V) across the DC link, current (A) through the load and power (W) delivered to the load across the capacitor at different wind velocity conditions (change in speed from 7 m/s to 6 m/s and then to 5 m/s)
- Fig. 6.1 Variations in the SRG output for different combinations of  $\theta_{on}$  and  $\theta_{off}$  at a constant excitation voltage of 100V and a wind speed of 10 m/s
- Fig. 6.2 Variation of SRG output power for fixed combinations of  $\theta_{on}$  and  $\theta_{off}$  at three different wind speeds at different applied voltages
- Fig. 6.3 Flow charts for the optimization techniques: (a) GSA (b) PSO
- Fig. 6.4 Voltage, flux, current and torque of the SRG whose  $\theta_{on}$  and  $\theta_{off}$  are optimized by PSO at generator speeds of (a) 1350 rpm (wind speed 9 m/s), (b) 1250 rpm (wind speed 8 m/s), (c) 1140 rpm (wind speed 7 m/s) and (d) Speed, voltage and power at different wind speeds.
- Fig. 6.5 Voltage, flux, current and torque of the SRG whose  $\theta_{on}$  and  $\theta_{off}$  are optimized by GSA at generator speeds of (a) 1350 rpm (wind speed 9 m/s), (b) 1250 rpm (wind speed 8 m/s), (c) 1140 rpm (wind speed 7 m/s) and (d) Speed, voltage and power at different wind speeds

- Fig. 6.6 DC-DC converters: (a) Cuk, (b) Zeta, (c) Landsman and (d) SEPIC
- Fig. 6.7 DC-DC converters: (a) Output voltage ripple content, (b) Output current ripple content, and (c) Switch stress
- Fig. 6.8 Phase 1 and 3 voltages and currents of SRG at a speed of 1200 rpm
- Fig. 6.9 Phase 1 and 3 voltages and currents of SRG at a speed of 1300 rpm
- Fig. 6.10 Phase 1 and 3 voltages and currents of SRG at a speed of 1650 rpm
- Fig. 6.11 Inductor 1 & Inductor 2 currents of the SEPIC, output voltages of the SRG and the SEPIC (at a speed of 1200 rpm)
- Fig. 6.12 Inductor 1 & Inductor 2 current of the SEPIC, output voltages of the SRG and the SEPIC (at a speed of 1300 rpm)
- Fig. 6.13 Inductor 1 & Inductor 2 current of the SEPIC, output voltages of the SRG and the SEPIC (at a speed of 1650 rpm)
- Fig. 6.14 Inductor 1 & Inductor 2 currents, voltage stresses across the switch & diode of the SEPIC (at a speed of 1200 rpm)
- Fig. 6.15 Inductor 1 & Inductor 2 currents, voltage stress across the switch & diode of the SEPIC (at a speed of 1300 rpm)
- Fig. 6.16 Inductor 1 & Inductor 2 currents, voltage stress across the switch & diode of the SEPIC (at a speed of 1650 rpm)
- Fig. 6.17 Variations in the output voltages and output power of the SRG and SEPIC with change in speed
- Fig. 6.18 Battery voltage and battery current while the battery is charging (at a generator speed of 1650 rpm and at an output voltage of 120 V)
- Fig. 6.19 Battery voltage and battery current while the battery is discharging (to the load of  $24 \Omega$  when the wind speed is zero)
- Fig. 7.1 System configuration of the laboratory prototype of the SRG based WPGS
- Fig. 7.2 8/6 SRM along with rotor position marker that has graduations at every  $2^\circ$  interval
- Fig. 7.3 Rotary encoder (a) Fitted to the machine shaft, (b) Connections from the encoder to the DSP pins, (c) Pulses from A and B and Index terminals of the encoder for clockwise direction of rotation, (d) Pulses from A and B terminals of the encoder for counter-clockwise direction of rotation, (e) QEP A, QEP B and QEPI from the experimental setup and (f) Magnified image of QEPA, QEPB and QEPI from the experimental setup
- Fig. 7.4 DSPTMS320F28379D TI-DSP card
- Fig. 7.5 Sensor boards for sensing (a) Current and (b) Voltage
- Fig. 7.6 Circuit diagrams of AHBC, SEPIC and BDC with battery
- Fig. 7.7 Experimental set-up
- Fig. 7.8 Level Shifter, tapping inductor, film capacitor and battery bank
- Fig. 8.1 Voltage (Phase A), current (Phase A), speed and gate pulses (IGBTs of Phase A) for the closed loop control of SRM at three different speeds (157 rad./s, 188.5 rad/s and 167.5 rad./s)
- Fig. 8.2 Phase A voltage & current, speed and gate pulses (to the IGBTs of Phase A) during regenerative braking condition when the speed is reduced from 188.5 rad./s to 167.5 rad./s

- Fig. 8.3 Phase-Current and phase voltage in the regenerating condition
- Fig. 8.4 Phase voltage and current of the SRG at a speed of 1140 rpm
- Fig. 8.5 Phase voltage and current of the SRG at a speed of 1050 rpm
- Fig. 8.6 Phase voltage and current of the SRG at a speed of 920 rpm.
- Fig. 8.7 Phase C voltage (80 V), phase C current of the SRG at a speed of 1200 rpm with the conduction angle of  $0^\circ$  to  $22.5^\circ$
- Fig. 8.8 Phase C voltage (80 V), phase C current and rotor position (depicting periodicity of  $60^\circ$ ) at a speed of 1200 rpm
- Fig. 8.9 Voltage, current and speed waveforms at three different speeds: 1350 rpm, 1250 rpm and 1140 rpm
- Fig. 8.10 Voltage and current at a speed of 1350 rpm
- Fig. 8.11 Voltage and current at a speed of 1250 rpm
- Fig. 8.12 Voltage and current at a speed of 1140 rpm
- Fig. 8.13 Variations in the output power  $P_{dc}$ . (W) and reference power  $P_{ref}$ . (W) at three different speeds of 1350 rpm, 1250 rpm and 1140 rpm
- Fig. 8.14 Inductor 1 & 2 currents, output voltages of the SRG (80 V) and the SEPIC (48 V) at an SRG speed of 1200 rpm
- Fig. 8.15 Inductor 1 & 2 currents, switch and diode voltages of the SEPIC at an SRG speed of 1200 rpm
- Fig. 8.16 SRG Phase 1 current & voltage, Phase 3 current & voltage at a speed of 1200 rpm (generated voltage is 80 V)
- Fig. 8.17 Inductor 1 & 2 currents, output voltages of the SRG (90 V) and the SEPIC (48 V) at 1300 rpm speed
- Fig. 8.18 Inductor 1 & 2 currents, switch and diode voltages of the SEPIC at 1300 rpm speed
- Fig. 8.19 SRG Phase 1 current and voltage, Phase 3 current and voltage, at a speed of 1300 rpm (generated voltage is 90 V)
- Fig. 8.20 Phase 1 current and voltage of the SRG and output voltage at 1650 rpm speed (Generated voltage is 120 V)
- Fig. 8.21 Inductor 1 & 2 currents, switch and diode voltages of the SEPIC at an SRG output voltage of 120V and generator speed of 1650 rpm
- Fig. 8.22 Battery voltage and current while the battery is charging
- Fig. 8.23 SEPIC output voltage regulated to 48 V DC when the SRG output is varying from 80 V to 90 V and then to 120 V for three different speeds of 1200 rpm, 1300 rpm and 1650 rpm respectively

## **LIST OF TABLES**

Table 3.1	Name-plate details of the SRM
Table 4.1	Comparison of responses of different models for the SRM
Table 5.1	Simulated values of capacitor voltage ripples for different wind speeds
Table 6.1	Different parameters of the SRG based WPGS while employing GSA
Table 6.2	Different parameters of the SRG based WPGS while employing PSO
Table 6.3	Different parameters of the SRG based WPGS without using any optimization algorithm
Table 6.4	Comparison among dc-dc converter topologies for an SRG based WPGS



## LIST OF ABBREVIATIONS

ADC	Analog digital converter
AHBC	Asymmetric half bridge converter
BDC	Bi-directional converter
BESS	Battery energy storage system
DAC	Digital to Analog Converter
DFIG	Doubly fed induction generator
DSP	Digital Signal Processor
DTC	Direct Torque Control
ePWM	Enhanced Pulse Width Modulation
eQEP	Enhanced Quadrature Encoder Pulse
EV	Electric Vehicle
GPIO	General Purpose Input Output
IGBT	Insulated Gate Bipolar Transistor
MATLAB	Matrix Laboratory
MPPT	Maximum power point tracking
PI	Proportional-Integral
PMBLDC	Permanent magnet brushless dc motor
PMSG	Permanent magnet synchronous generator
PPR	Pulses Per Revolution
PWM	Pulse Width Modulation
RMS	Root Mean Square
RPM	Revolutions per minute
SEPIC	Single ended primary inductor converter
SRG	Switched reluctance generator
SRM	Switched reluctance motor
VSI	Voltage Source Inverter
WECS	Wind energy conversion system
WPGS	Wind power generating system



## LIST OF SYMBOLS

$E_b$	Back EMF of the motor (V)
$f$	Frequency of applied ac voltage (Hz)
$f_{clk}$	DSP system clock frequency (Hz)
$f_{sw}$	Inverter switching frequency (Hz)
$I_{ref.}$	Reference current (A)
$i_{ph}$	Phase current (A)
$J$	Motor inertia (kg-m <sup>2</sup> )
$K_{opt}$	Proportionality constant for wind turbine characteristics
$K_p$	Proportionality constant of the PI controller
$K_i$	Integral constant of the PI controller
$L_a$	Aligned inductance (H)
$L_u$	Un-aligned inductance (H)
$P$	Number of poles
$P_{dc}$	DC output power (W)
$P_{ref.}$	Reference power (W)
$P_{out}$	Average output power (W)
$R_{ph}$	Stator per phase resistance ( $\Omega$ )
$T_e$	Electromagnetic torque (Nm)
$T_L$	External load torque (Nm)
$V_s$	Supply voltage
$V_{ph}$	Phase voltage (V)
$\Omega$	Speed (rpm)
$\omega_e$	Rotor speed (electrical rad/sec)
$\omega_m$	Mechanical rotor speed (rad/sec)
$\theta$	Rotor position (degree)
$\theta_{on}$	Turn-on angle (degree)
$\theta_{off}$	Turn-off angle (degree)
$\theta_{tot}$	Total Angle (degree)
$\theta_{ext}$	Extinction angle (degree)
$\varphi$	Flux linkage (Weber)

